Early controlled release of peroxisome proliferator-activated receptor β/δ agonist GW501516 improves diabetic wound healing through redox modulation of wound microenvironment.

Xiaoling WANG[1#], Ming Keat SNG[1#], Selin FOO[1], Han Chung CHONG[1], Wei Li LEE[2], Mark Boon Yang TANG[3], Kee Woei NG[2], Baiwen LUO[2], Cleo CHOONG[2], Marcus Thien Chong WONG[4], Benny Meng Kiat TONG[5], Shunsuke CHIBA[5], Say Chye Joachim LOO[2], Pengcheng ZHU[1*], Nguan Soon TAN[1,6*]

[1]School of Biological Sciences, Nanyang Technological University, 60 Nanyang Drive, Singapore 637551.
[2]School of Materials Science and Engineering, Nanyang Technological University, Singapore 639798.
[3]National Skin Centre, 1 Mandalay Road, Singapore 308205.
[4]Tan Tock Seng Hospital, 11 Jalan Tan Tock Seng, Singapore 308433.
[5]Division of Chemistry and Biological Chemistry, School of Physical and Mathematical Sciences, Nanyang Technological University, 21 Nanyang Link, Singapore 637371.
[6]Institute of Molecular and Cell Biology, 61 Biopolis Drive, Proteos, Singapore 138673.

[#]Authors contributed equally

*Co-corresponding authors:
PZ: pczhu@ntu.edu.sg
NST: nstan@ntu.edu.sg or nstan@imcb.a-star.edu.sg; Tel: +65-6316-2941; Fax: +65-67913856

Keywords
Diabetic wound healing, Hydrogen peroxide, Microparticle, Peroxisome proliferator-activated receptor beta/delta, Controlled release, GW501516.

ABSTRACT

Diabetic wounds are imbued with an early excessive and protracted reactive oxygen species production. Despite the studies supporting PPARβ/δ as a valuable pharmacologic wound healing target, the therapeutic potential of PPARβ/δ agonist GW501516 (GW) as a wound healing drug was never investigated. Using topical application of polymer-encapsulated GW, we revealed that different drug release profiles can significantly influence the therapeutic efficacy of GW and consequently diabetic wound closure. We showed that double-layer encapsulated GW microparticles (PLLA:PLGA:GW) provided an earlier and sustained dose of GW to the wound and reduced the oxidative wound microenvironment to accelerate healing, in contrast to single-layered PLLA:GW microparticles. The underlying mechanism involved an early GW-mediated activation of PPARβ/δ that stimulated GPx1 and catalase expression in fibroblasts. GPx1 and catalase scavenged excessive H_2O_2 accumulation in diabetic wound beds, prevented H_2O_2-induced ECM modification and facilitated keratinocyte migration. The microparticles with early and sustained rate of GW release had better therapeutic wound healing activity. The present study underscores the importance of drug release kinetics on the therapeutic efficacy of the drug and warrants investigations to better appreciate the full potential of controlled drug release.

1. Introduction

Diabetes is a complex metabolic disorder that may cause both acute and long-term complications, severely affecting ~200 million people worldwide [1]. One of the most debilitating complications in diabetes is refractory wound healing, resulting in severe complications that frequently cause morbidity and mortality [1]. About 15% of diabetic patients have an impaired, non-healing wound [2], among which 81% has been attributed to diabetic amputations [3]. A better knowledge of diabetic wound pathology would lead to new therapeutic targets, more efficient wound management and eventually improved diabetic patient well-beings [4].

Normal wound healing involves intricate communications among different cell types and their interactions with the wound microenvironment. These cells, through the release of numerous growth factors, cytokines and chemical mediators, regulate and coordinate the healing process via a series of events including inflammation, re-epithelialization and matrix remodelling [5]. An important chemical mediator is reactive oxygen species (ROS). A proper redox control of the wound microenvironment is essential for different stages of normal wound healing process [6-8]. Under normal conditions, a delicate balance of free radicals has antimicrobial and pro-mitogenic functions that are essential to wound healing [9, 10]. Large amount of ROS produced by inflammatory cells during early-phase of wound healing, until post-injury day 3, is essential to protect the wounded skin against invading pathogens [11]. Thereafter ROS level decreases and re-epithelialisation phase is initiated by migration of keratinocytes along the injured dermis. In contrast, poor healing diabetic wounds are often associated with a prolonged inflammatory stage and therefore a de-regulation on the time-dependent release of ROS in the wound microenvironment [7, 9, 11, 12]. An excessive and protracted ROS production and decreased free radical scavenging enzyme activities are linked to chronic hyperglycaemia in diabetic rodents [12]. Therefore, ROS regulation in wound healing especially in diabetic conditions warrants further study.

Numerous studies have shown that peroxisome proliferator-activated receptor β/δ (PPARβ/δ), a ligand-activated transcription factor, plays pivotal roles in wound healing. The activation of PPARβ/δ conferred an anti-apoptotic effect on the keratinocytes *in vivo*, hence protecting them from cytokine-induced apoptosis during the inflammatory phase of wound repair, thereby maintaining a sufficient number of viable migratory keratinocytes for the re-epithelialization phase of the wound-healing process [13-15]. PPARβ/δ also induces the expression of pro-angiogenic angiopoietin-like 4 (ANGPTL4) and secreted interleukin-1 receptor antagonist (sIL-1ra) to influence wound angiogenesis, scar formation and tissue remodelling [16, 17]. Despite the existing studies potentiating PPARβ/δ as a valuable pharmacologic wound healing target, affecting many events in all phases of wound healing [18, 19], the roles of PPARβ/δ in regulating ROS in wound microenvironment and in diabetic wound healing remain unclear. Moreover, the clinical impact of a PPARβ/δ agonist as a pharmacological agent for the treatment of diabetic wounds has not been investigated.

In recent years, the study of controlled release of drugs and bioactive agents from polymeric materials and microparticulate drug carriers to a given target has been of great scientific interest. Controlled release formulations can be used to reduce the amount of drug necessary to provide the same therapeutic effect in patients. Another undoubted advantage is also improved patient compliance. Over the years of controlled release research, different systems, ranging from coated tablets, gels to biodegradable microspheres and osmotic systems have been explored to get predesigned release profiles. In the past two decades, poly(L-lactide) (PLLA) and poly(D,L-lactide–co-glycolide) (PLGA) have been among the most attractive polymeric candidates used to fabricate devices for drug delivery and tissue engineering applications. They are biocompatible and biodegradable, exhibit a wide range of

erosion times, have tuneable mechanical properties and most importantly, are FDA approved polymers [20-24]. However, there is little literature examining the *in vivo* biological outcome of controlled delivery of drugs with different release kinetic profiles. In this study, we examine the biological impact of different controlled release of PPARβ/δ agonist GW501516 (IUPAC: {4-[({4-methyl-2-[4-(trifluoromethyl)phenyl]-1,3-thiazol-5-yl}methyl)sulfanyl]-2-methylphenoxy}acetic acid, abbreviated as GW hereafter) on healing of diabetic wounds and study their mechanism of action.

2. Materials and Methods

2.1. Materials.

Poly(L-lactide) (PLLA) (intrinsic viscosity (IV): 2.38, Bio Invigor), poly(D,L-lactide–co-glycolide, 50:50) (PLGA) (IV: 1.18, Bio Invigor) and poly(vinyl alcohol) (PVA) (MW: 30-70 kDa, Sigma-Aldrich) were used without further purification. Dichloromethane (DCM) from Tedia Company Inc. was of high-performance liquid chromatography (HPLC) grade and used as received. Luciferase® Reporter Assay System and Fugene® HD Transfection Reagent (Promega, USA). SuperFrost Plus slides (Thermo Fisher Scientific). iScript™ cDNA Synthesis kit (Bio-Rad). SYBR Green PCR Master Mix (Applied Biosystem, CA). Monoclonal anti-PPARβ/δ antibody (Millipore).

2.2. Microencapsulation of GW.

GW-loaded double-layered PLLA-PLGA (core-shell) microparticles were prepared using the oil-in-water (o/w) emulsion solvent evaporation method [25, 26]. Briefly, the two polymers (67 mg of PLGA, 33 mg of PLLA) and GW501516 (1 mg) were dissolved in 1.33 mL DCM. This solution was then poured into the 250 mL of PVA aqueous solution (0.5% w/v). The emulsion was stirred at 2000 rpm using an overhead stirrer (Calframo BDC1850-220) at room temperature (25 ºC). The evaporation of DCM gave rise to phase separation of PLGA and PLLA, yielding double-layered microparticles (designated as PLLA:PLGA:GW hereafter). Lastly, the particles were centrifuged, rinsed with deionised water, lyophilised and stored in a desiccator for further characterization. GW501516-loaded single-layered PLLA (designated as PLLA:GW hereafter) or PLGA microparticles (designated as PLGA:GW hereafter) were similarly prepared whereby 100 mg of polymer (PLLA or PLGA) was used. Vehicle control microparticles were made with similar process parameters as above whereby no GW was encapsulated.

2.3. Determination of polymer distribution.

Raman mapping was utilized to verify the polymer distribution within the microparticles. Microparticles that had been pre-sectioned were placed under a microscope objective with a laser power of up to a ~20 mW. Raman point-by-point mapping measurements were performed in both x and y directions using a Raman microscope (In-Via Reflex, Renishaw) equipped with a near-infrared enhanced deep depleted thermoelectrically Peltier-cooled CCD array detector (576×384 pixels) and a high-grade Leica microscope. The sample was irradiated with a 785 nm near-infrared diode laser, and an objective lens was used to collect the backscattered light. Measurement scans were collected using a static 1800-groove-per-mm dispersive grating in a spectral window from 300 to 1900 cm^{-1}, and the acquisition time for each spectrum was approximately 35 s. Raman mapping data were further analysed using the band target entropy minimization (BTEM) algorithm to reconstruct pure component spectral estimates.

2.4. Electron microscopy of the microparticles.

The surface and internal morphologies of the microparticles were viewed using scanning electron microscopy (SEM, JSM-6360) at 5 kV. Before analysis, the samples were mounted onto a metal stub and submerged in liquid nitrogen before chopped with a razor blade. Samples were subsequently coated with gold using a sputter coater (SPI-Module).

2.5. Drug encapsulation efficiency

Encapsulation efficiency is defined as the ratio of actual to theoretical drug loading within the microparticles. For quantification of GW loading, 5 mg of microparticles were added into 1 ml of 1 M NaOH solution and incubated for 24 h at 37 $^{\circ}$C. The mixture was then centrifuged and supernatant drawn. The concentration of GW501516 was determined using a UV-Vis spectrophotometer (Shimadzu UV-2501) at 318 nm. All measurements were done in triplicate.

2.6. In vitro GW release kinetic assay

In vitro GW release kinetic assay was performed using a rotating system. Briefly, 50 ng of GW-loaded microparticles were re-suspended in 1 ml of saline and kept in the rotating system for continuous release of GW from the microparticles at 37 ^{o}C. On a daily basis, 10 µl of the supernatant was used to measure the concentrations of GW on a UV-Vis spectrophotometer (Shimadzu UV-2501) at 318 nm. All measurements were done in triplicate. The assay was carried out up to 12 days.

2.7. Transfection and luciferase assay.

Drug release study was performed as previously described, except that serum-free culture medium was used [27]. HEK293T cells were co-transfected with PPRE-tk-luciferase reporter vector and pCDNA3.1-PPARβ/δ using Fugene® HD Transfection Reagent (Promega, USA). RL Renilla luciferase control reporter vector was used as a control for transfection efficiency. The next day, medium was aspirated and replaced with conditioned medium were collected daily for luciferase assay for a period of 10 days. Luciferase assay was performed using Dual Luciferase® Reporter Assay System (Promega, USA) and the Glomax 20/20 Luminometer (Promega, USA) to monitor drug release kinetics and biological activity of released GW501516.

2.8. Measurement of reactive oxygen species (ROS)

Extracellular H_2O_2 was measured using Amplex Red Hydrogen Peroxide/Peroxidase assay kit (Life Technologies) as described by manufacturer. Briefly, 5 x 10^4 fibroblasts, macrophages or keratinocytes were incubated with 50 µM Amplex Red reagent (10-acetyl-3,7-dihydroxyphenoxazine) and 0.1 U/ml horseradish peroxidase (HRP) in Krebs-Ringer phosphate buffer for 1 h at 37 °C. Next, cells were removed by centrifugation and resorufin fluorescence in the supernatant was measured at emission of 590 nm (excitation 485 nm) using Tecan SPECTRAFlour Plus (Tecan Systems) plate reader. Results were reported in arbitrary fluorescence units. For intracellular ROS measurement, 5 x 10^4 cells of interest were incubated with 10 µM 5-(and 6-) chloromethyl-2′,7′-dichlorodihydrofluorescein diacetate, acetyl ester fluorophores (CM-H2DCFDA, Life Technologies) for 30 min at 37°C. Next, cells were detached and analysed by Accuri C6 Flow cytometer (BD). ROS in wound fluid was measured using 20 µl of wound fluid in a 200 µl Amplex Red final reaction volume. Wound fluid was collected as previously described [14]. Amplex Red conversion to resorufin fluorescence was measured as described above.

2.9. In vitro catalase and GPx activities assays

Fibroblasts (10^6 per treatment) were seeded overnight and treated with indicated concentrations of GW501516 for 6 h. Catalase and GPx activities were measured according to the Amplex Red Catalase Assay Kit (Molecular Probes) and the Glutathione Peroxidase Assay Kit (Abcam) manufacturers' protocols, respectively. Cell protein concentrations were used for final normalization. Each experiment was repeated twice with triplicates.

2.10. In vivo wound healing experiments.

Diabetic (db/db) and wild-type control (db/+) male mice of 6-8 weeks old were purchased from The Jackson Laboratory. Criteria for inclusion were a blood glucose level of less than 200 mg/dl (control, db/+) or over 300 mg/dl (diabetic, db/db). Two full-thickness excisional splint wounds were inflicted on the dorsal skin of each mouse as previously described [28]. GW (1 ng) or GW (1 ng)-loaded microparticles (PLGA:GW, PLLA:GW or PLLA:PLGA:GW) were re-suspended in saline and topically applied onto one wound. Control experiments were carried out accordingly using vehicle DMSO alone, PLGA:veh, PLLA:veh or PLLA:PLGA:veh on the other wound. Finally, the wounds were covered with 3M™ Tegaderm transparent film dressing to prevent leakage of the microparticles or solution. Wound closure was measured daily in a double-blinded manner until end of experiment. Animals were sacrificed on days 3, 5, 7, 9 and 10 post wounding. Wound biopsies were harvested, centrally bisected and subjected to histology staining for measurement of the epithelial tongue length and wound epithelial area. At least 5 animals were used for each individual treatment at every single time point. All animals were maintained in specific pathogen-free conditions. The animal studies were approved by the Institutional Animal Care and Use Committee (ARF-SBS/NIE- A0174AZ).

2.11. In vitro wound healing assay.

Rat tail type I Collagen (BD Biosciences) was used to coat a 24-well-plate (Corning Life Sciences) at a concentration of 50 μg/cm^2 for 1 h at 25 ^{o}C. PBS-diluted hydrogen peroxide (H_2O_2) with varied concentrations was used to treat the pre-coated plate for 3 h at room temperature, and the plate was washed thrice with PBS and dried. Individual silicone insert (Ibidi Pte Ltd), with a defined cell-free gap (500 μm ± 50 μm), was placed and attached into each well of the pre-treated plate. 1 x 10^4 of keratinocytes were seed into individual well of each silicone insert. Cells were allowed to attach for 12 h before the insert was gently removed. Cells were replenished with fresh media and cultured in the Cell-IQ machine (CM technologies) for real-time photographing as the cells migrate and cover the cell-free gap. Wound healing rate was assessed using the Cell-IQ analysis software (CM Technologies).

2.12. Statistical Analysis.

Statistical analyses were performed using Mann-Whitney test using SPSS v.19 software (IBM Corporation, USA). A p value of <0.05 was considered significant.

3. Results

3.1 PPARβ/δ activation kinetics of PLLA:GW, PLGA:GW and PLLA:PLGA:GW.

To achieve different release kinetics, PPARβ/δ agonist GW was encapsulated in single-layered PLLA and double-layered PLLA:PLGA microparticles. Raman mapping of PLLA:PLGA:GW showed that PLGA and PLLA abundantly distributed in shell and core regions, respectively (Fig. 1a); PLGA spread evenly all over PLLA:GW as shown in the cross-sectional view of PLLA:PLGA:GW microparticles (Fig. 1b). Both types of

microparticles, diameters ranging from 75-125 μm, possessed spherical shapes with smooth surfaces (Fig. 1b, upper panels). Cross-sectioning SEM micrographs revealed double- and single-layered structures of PLLA:PLGA:GW and PLLA:GW, respectively (Fig. 1b, lower panels). The average drug loading (weight) in the encapsulated microparticles was determined to be 0.07±0.005%, 0.065±0.005% and 0.2±0.014% for PLGA:GW, PLLA:GW and PLLA/PLGA:GW, respectively.

Next, to examine the release kinetics of encapsulated GW from these microparticles, we performed *in vitro* release study over a period of day 10 days. The released GW was detected by UV 318 nm absorbance. Results showed two distinctive GW release profiles by PLLA:PLGA:GW, PLLA:GW and PLGA:GW. GW was released rapidly from PLLA:PLGA:GW, peaked within 6 days, and thereafter sustained until day 10 (Fig. 1c). In contrast, GW was released slower from PLLA:GW and PLGA:GW for the first 7 days, followed by a drastic increase to its peak by day 10 (Fig. 1c). However, the *in vitro* acellular release study does not provide evidence about the biological activity of GW after encapsulation process. Thus, we performed a transient transactivation study using HEK 293T cells co-transfected with a PPARβ/δ expression vector and a luciferase reporter vector. We observed two PPARβ/δ activation profiles. PLLA:PLGA:GW rapidly increased the transactivation activity of PPARβ/δ when compared to PLLA:GW, reaching a sustained level by day 7 (Fig. 1d). PLLA:GW and PLGA:GW weakly activated PPARβ/δ at early time points, and showed rapid increase at day 7 post-transfection (Fig. 1d). No significant difference was detected between PLLA:GW and PLGA:GW at most of the time points. The transient transfection study used ectopic expression of PPARβ/δ via a mammalian expression vector. To study the drug efficacy of the microparticle-released GW on endogenous cellular level of PPARβ/δ, we examined the expression of two known PPARβ/δ target genes *ANGPTL4* and *sIL-1ra* in keratinocytes and fibroblasts, respectively [17, 29]. Consistent with the characteristic PPARβ/δ activation profiles obtained using HEK 293T, PLLA:PLGA:GW, PLLA:GW and PLGA:GW significantly increased ANGPTL4 expression in keratinocytes and sIL-1ra expression in fibroblasts, respectively (Fig. 1e-f). Their expression profiles were found to be regulated in a pattern similar to the drug release kinetic and PPARβ/δ activation profiles of PLLA:PLGA:GW, PLLA:GW and PLGA:GW (Fig. 1c-f). Cognate control drug-free microparticles PLLA:PLGA:veh, PLLA:veh and PLGA:veh showed no measurable transactivation activity even after 9 days post-transfection (Fig. S1a). Taken together, the single-layered (PLLA:GW and PLGA:GW) and double-layered (PLLA:PLGA:GW) microparticles showed delayed and early PPARβ/δ activation profiles, respectively.

3.2 Topical application of GW-loaded microparticles accelerates diabetic wound closure.

Next, we tested the effect of release-controlled microparticles as pharmacological agents for the treatment of diabetic wounds, on the re-epithelialization of full-thickness excisional splinted wounds in diabetic mouse. Mice were randomly divided into four groups, and topically treated with either PLGA:GW, PLLA:GW, PLLA:PLGA:GW or non-encapsulated GW along with their cognate vehicle controls. Consistent with the known beneficial roles of PPARβ/δ in wound healing, mice treated with non-encapsulated GW accelerated wound healing. Wound healing rate was faster in non-encapsulated GW-treated wounds from day 5 post-wounding when compared to vehicle treatment. However, the healing rate was transiently slower when compared to wounds treated with single-layered microencapsulated GW (Fig. S1b-c). Non-encapsulated GW-treated wounds also closed slower than PLLA:PLGA:GW treatment.

Both GW-loaded microparticles accelerated wound healing in diabetic mice, albeit with different efficacies. Notably, wounds treated with PLLA:PLGA:GW closed within 7 days (Fig. 2a-b), which was significantly faster than PPLA:PLGA:veh, PLLA:GW,

PLGA:GW and non-encapsulated GW (Fig. 2a-b). To gain further insight, we performed histomorphometric analyses of wound biopsies (Fig. 2c-d). From day 3 post wounding, PPLA:PLGA:GW-treated wound epithelia were significantly longer and thicker than PPLA:PLGA:veh-treated wounds (Fig.2c-d). In contrast, wounds treated with PLLA:GW or PLGA:GW closed only marginally faster than PPLA:veh (PLLA:GW vs PLLA:veh: 9 vs 10 days) and PLGA:veh (PLGA:GW vs PLGA:veh: 9 vs 10 days) (Fig. 2a). This was associated with a slightly longer and thicker neo-epithelial layer covering the area between the wound site and the margin of the regenerating tissue (Fig. 2c-2d). Our observations suggest that the two different release kinetics of GW have different efficacies in accelerating wound healing.

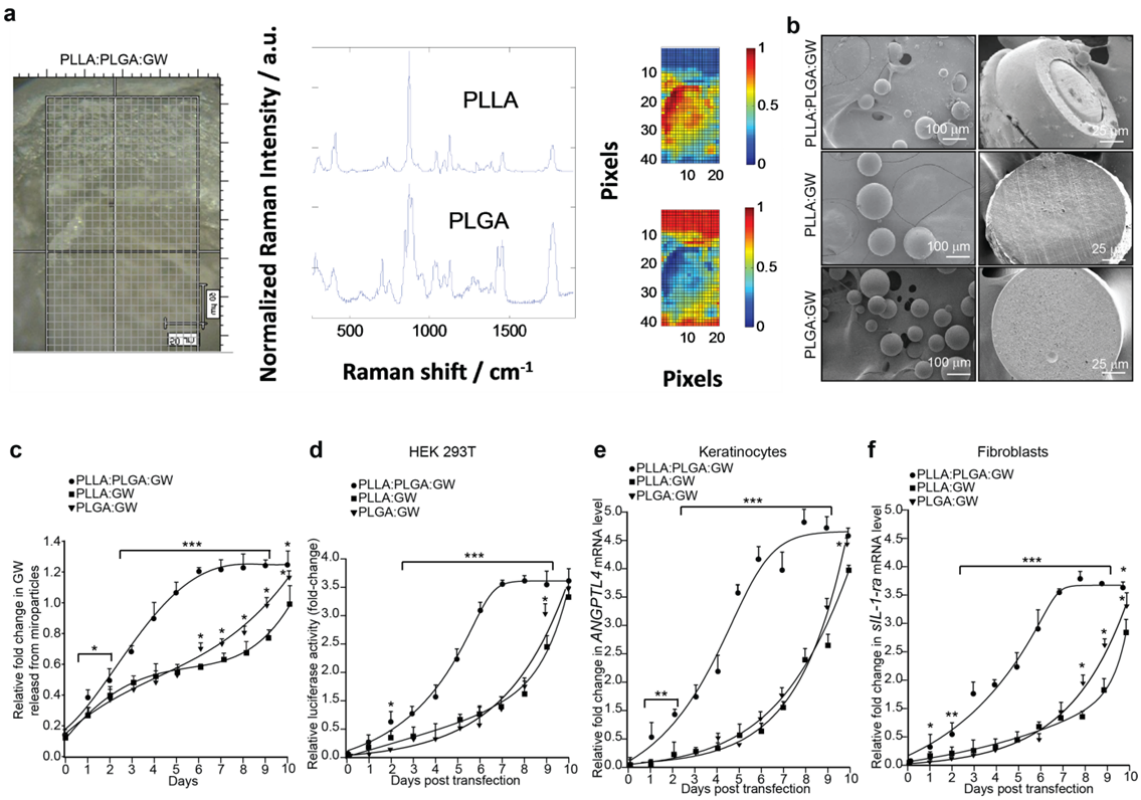

Fig. 1. Properties of GW encapsulated microparticles. (a) Raman mapping of PLLA:PLGA:GW. Colour intensity scale indicates relative polymer concentration. (b) SEM graphs of microparticles. (c) In vitro drug release kinetics of microparticles measured in saline. (c) Drug release kinetics of microparticles measured in HEK 293T. Relative luciferase activities were normalized to Renilla luciferase activities. (e, f) *ANGPTL4* (e) and *sIL1-ra* (f) mRNA expressions at indicated time points in keratinocyte and fibroblast, respectively. L27 was internal reference gene. (c-f) Data (means±SD) from 3 independent experiments with at least triplicates of each sample. * denotes $p<0.05$, ** for $p<0.01$ and *** for $p<0.001$ compared to PLLA:GW at corresponding time point.

3.3 PPARβ/δ activation modulates oxidative stress in diabetic wound.

Early controlled release of GW via PPLA:PLGA:GW microparticles significantly accelerated diabetic wound closure, while delayed release of GW by PPLA:GW and PLGA:GW exhibited marginal improvement to the re-epithelialization. To understand the mechanism for the difference in efficacy, we chose day 3 and day 5 wound biopsies from PLLA:PLGA:GW- and PLLA:PLGA:veh-treated mice and subjected them to microarray analysis. Interestingly, comparative gene expression analysis between the samples revealed genes involved in cellular oxidative stresses to be consistently altered (Fig. S2a and Table S1). As expected, we also noticed changes in the expression of a cluster of immune responsive

genes (Fig. S2b and Table S2). A study of wild-type wounds showed that ROS level in normal non-diabetic wounds decreased significantly (Fig. 2e), which coincided with the resolution of inflammation and the commencement of re-epithelialization. The ROS level in diabetic wounds remained significantly higher compared with wild-type wounds over the whole experimental period (Fig. 2e). Interestingly, wounds treated with PLLA:PLGA:GW showed significantly reduced ROS level, reaching a level closer to that of wild-type wounds (Fig. 2e). Next, we showed that wound fluid levels of H_2O_2 were significantly higher in diabetic mouse as compared with wild-type counterparts on day 3 and 5 post wounding as determined by a H_2O_2-sensitive Amplex Red assay (Fig. 2f). These observations suggest that GW may improve diabetic wound closure by reducing H_2O_2 level of the wound microenvironment.

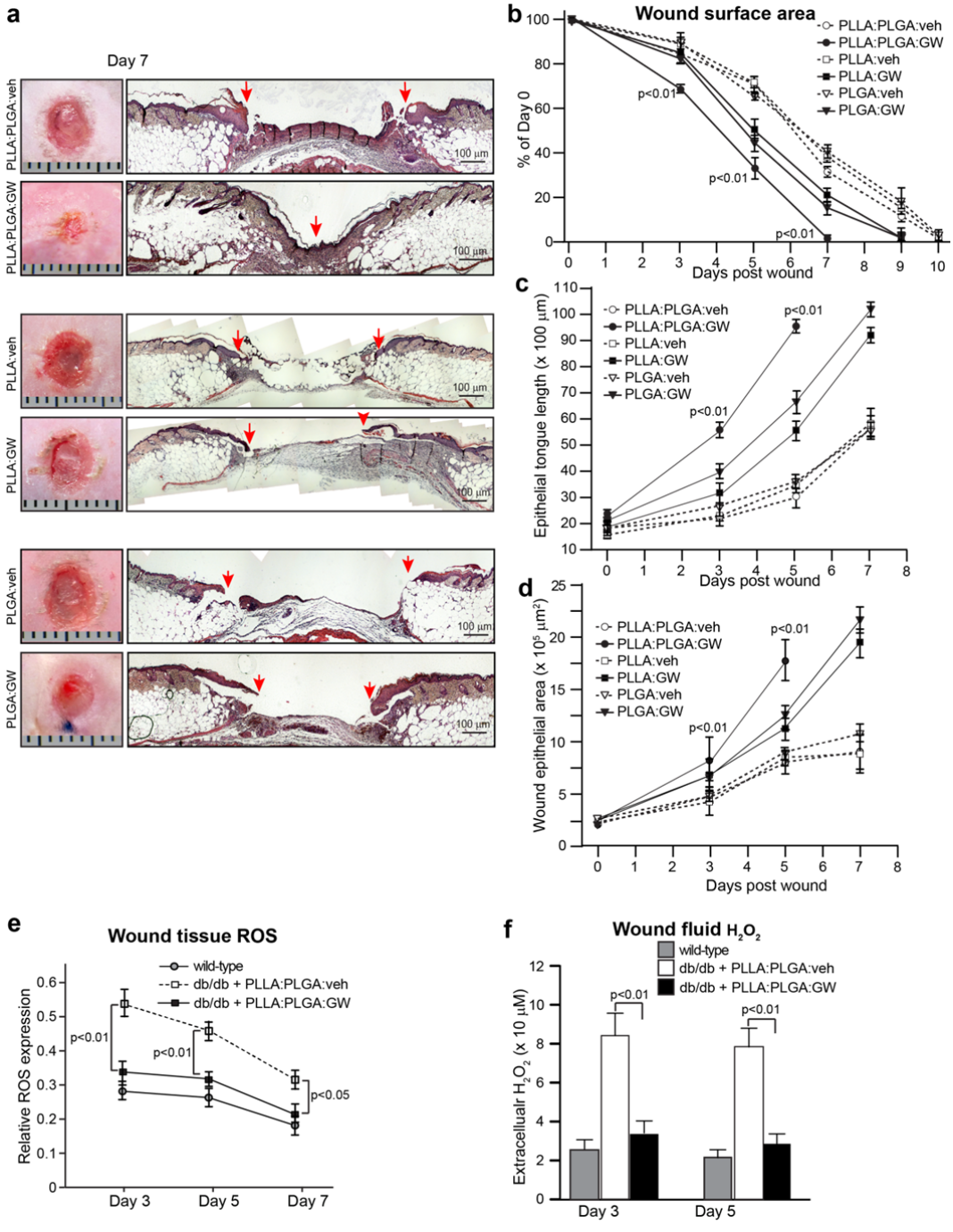

Fig. 2. Effects of GW loaded microparticles on diabetic wound healing. (a) Representative macroscopic wounds (left) and H&E (right) sections of diabetic wounds from indicated test groups (n ≥ 5) at day 7. Ruler units are in mm. Red arrows point to epithelial wound edge. (b) Wounds closure kinetics of mice treated with indicated GW- and vehicle-loaded microparticles. Wound surface area are plotted as percentage of day 0 (=100%). (c, d) Wound tongue length (c) and epithelial area (d) determined as previously described [28]. PLLA:PLGA:GW-treated wounds have completely re-epithelialized at day 7 post-wounding. Values (means ± SD) of 10 centrally dissected sections were from at least 5 mice. P values based on comparisons between PLLA:PLGA:GW treatment and cognate PLLA:PLGA:veh. (e) Relative ROS levels of wound tissues as measured by DCF. (f) H_2O_2 levels measured by Amplex Red on wound fluids from indicated time points. Data (means ± SD) from 5 independent experiments with at least triplicates of each sample.

3.4 H_2O_2-modified collagen delays keratinocyte migration.

A corrupted or damaged extracellular matrix (ECM) directly impairs cell-matrix communication, delays cell migration and thus the healing process. Therefore we proposed that excessive H_2O_2 might affect diabetic wound healing by acting as an oxidant that provisionally modifies wound ECM. To test this hypothesis, we examined the direct effect of H_2O_2-treated collagen on cell migration using a modified *in vitro* wound assay. Culture plate coated with a thin layer of rat tail type I collagen was treated for 3 h with various concentrations of H_2O_2. The residual H_2O_2 was thoroughly washed off with phosphate buffered saline. To determine if H_2O_2 can modify collagen, we performed a Fourier transform infrared spectroscopy (FTIR) analysis on H_2O_2-treated collagen. FTIR results confirmed that several amide positions were modified by H_2O_2 when compared with vehicle treatment (Fig. 3a). Next, we performed *in vitro* keratinocyte wound assay on H_2O_2-treated collagen coated plate. Interestingly, we observed that wound closure rate was significantly reduced on H_2O_2 (10 μM and 100 μM) pre-treated collagen compared with vehicle pre-treated collagen (Fig. 3b and S3a). H_2O_2 treatment (10-100 μM) showed little effect on keratinocyte apoptosis (Fig. 3c and S3b) or proliferation (Fig. 3d and S3c). These observations indicate that the modification of collagen by H_2O_2 retards *in vitro* wound healing through reducing keratinocyte migration rate.

3.5 PPARβ/δ activation diminishes H_2O_2 secretion from diabetic fibroblasts.

The extracellular redox state of wound microenvironment is determined at least in part by the intracellular redox state in the surrounding cells. Thus, to understand how PPARβ/δ agonist GW may directly modulate the redox state of the wound microenvironment, we first determine the major producer of H_2O_2 in the diabetic wounds. We measured the intracellular and extracellular H_2O_2 levels of the three major skin cell types- fibroblast, keratinocyte, and macrophage, maintained in diabetic culture conditions [30]. Fibroblasts produced significantly more intracellular and extracellular H_2O_2 as compared to the other two cell types (Fig. 4). Importantly, GW treatment dose-dependently decreased both intra- and extra-cellular H_2O_2 levels in fibroblasts (Fig. 4). As expected, macrophages also showed a similar trend upon GW treatment, albeit with a much lower starting H_2O_2 level (Fig. 4). GW has no significant effect on H_2O_2 production in keratinocyte (Fig. 4). Next, to determine whether the effect of GW was mediated by PPARβ/δ, we used PPARβ/δ antagonist GSK0660 (IUPAC: methyl 3-({[2-(methoxy)-4 phenyl]amino}sulfonyl)-2-thiophenecarboxylate, abbreviated as GSK herein) and PPARβ/δ inverse agonist compound 10h (IUPAC: methyl 3-(N-(4-(isopentylamino)-2-methoxyphenyl)sulfamoyl)-thiophene-2-carboxylate, abbreviated as Cpd herein) [31, 32]. Both GSK and Cpd significantly reversed the effect of GW on H_2O_2 level in both fibroblasts and macrophages (Fig. 4), indicating that the effect of GW on H_2O_2 level was mediated via PPARβ/δ.

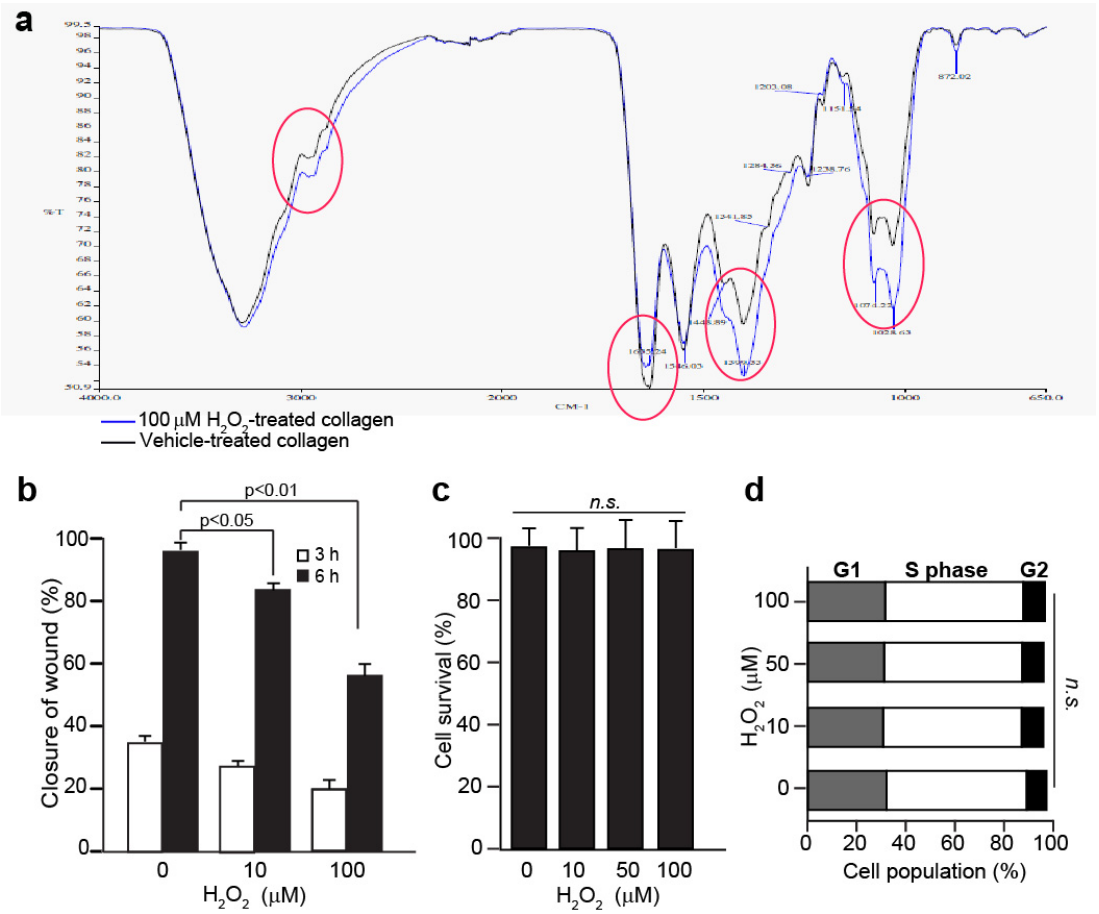

Fig. 3. H_2O_2 modulates collagen to retard in vitro wound closure. (a) FITR spectra of collagen with indicated treatments. Spectral differences between the two treatments were highlighted in red circles. (n = 4). (b) *In vitro* scratch wound closure kinetic by keratinocytes. Wound closure as percentage of time 0 width (= 100% is 500 μm). Representative time-lapsed images as shown in Fig. S3a. Effects of H_2O_2 treatment on (c) cell survival (AV-/PI- population) and (d) proliferation (indicated as percentage of various cell cycle phases as measured by BrdU assay). Representative FAC plots are as shown in Fig. S3b and S3c. Data (means ± SD) from 5 independent experiments with at least triplicates of each sample. *n.s.* not significant.

3.6 GW-activated PPARβ/δ stimulates catalase and GPx1 expression.

To understanding the underlying mechanism, we performed a qPCR screening of the ROS-related genes of fibroblasts that were obtained by laser microdissection from wound biopsies. Our results revealed that *GPx1* and *catalase* were the major genes responsive to GW treatment (Fig. 5a), both of which are related to cellular H_2O_2 regulation. They were significantly increased in PLLA:PLGA:GW-treated wounds when compared with PLLA:PLGA:veh treatment (Fig. 5b). To strengthen our finding, we performed a transient knockdown of PPARβ/δ in fibroblasts using siRNA. PPARβ/δ.was successfully knockdown, which was further verified by the reduced expression of sIL-1ra, a target gene of PPARβ/δ. in fibroblasts, upon GW treatment (Fig. 5b). The up-regulation of GPx1 and catalase mRNA and activities by GW was nullified in PPARβ/δ-deficient fibroblasts (Fig. 5b-d). Consistently, PPARβ/δ-knockdown abolished H_2O_2-reducing effect by GW in fibroblasts (Fig. 5e), indicating that the effect of GW was PPARβ/δ-dependent. Finally, *in vitro* chromatin immunoprecipitation (ChIP) showed that PPARβ/δ specifically bound to the cognate responsive elements (PPREs) in different promoter regions of both human and mouse

catalase and *GPx1* genes in GW-treated but not vehicle-treated diabetic fibroblasts (Fig. 5f). No immunoprecipitation or amplification was seen with pre-immune IgG (p.i.) or with a control sequence upstream of PPRE regions (Fig. 5f). These observations indicate that *catalase* and *GPx1* are direct target genes of PPARβ/δ. Our findings suggest early controlled release of GW improves diabetic wound closure by reducing redox modifications of ECM due to excessive H_2O_2 production from diabetic wound fibroblasts and macrophages.

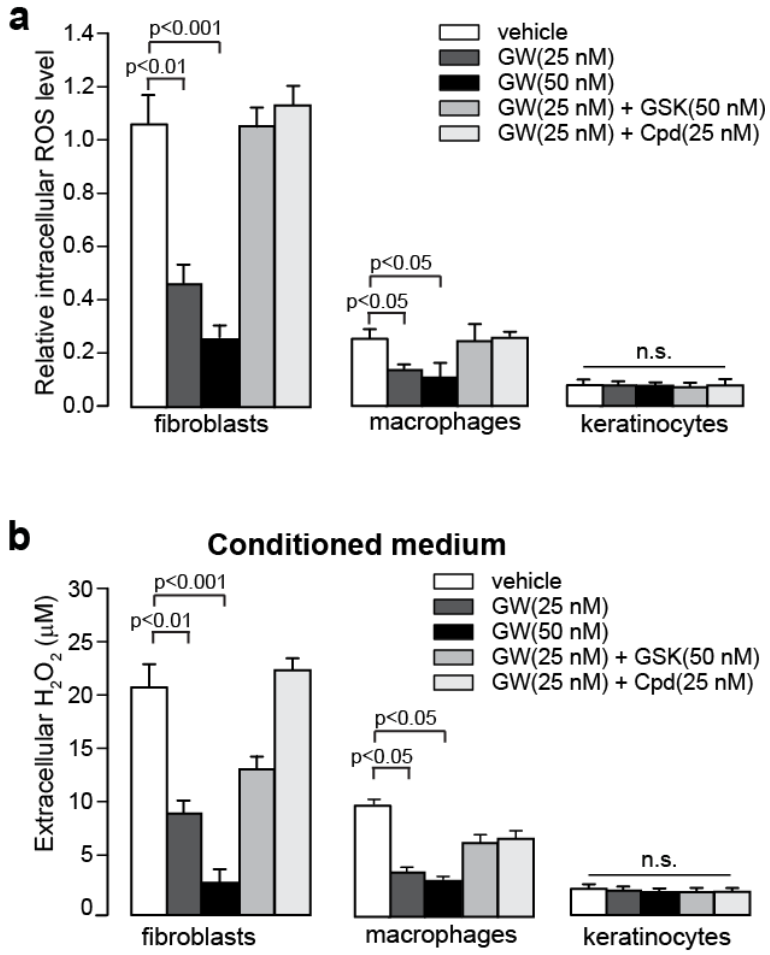

Fig.4. GW inhibits H_2O_2 production in fibroblasts and macrophages. (a) Intracellular H_2O_2 and (b) extracellular ROS levels 6 h post indicated treatments as measured by CM-H2DCFDA and Amplex Red reagents, respectively. Data (mean ± SD) from 3 independent experiments with at least triplicates. n.s. not significant.

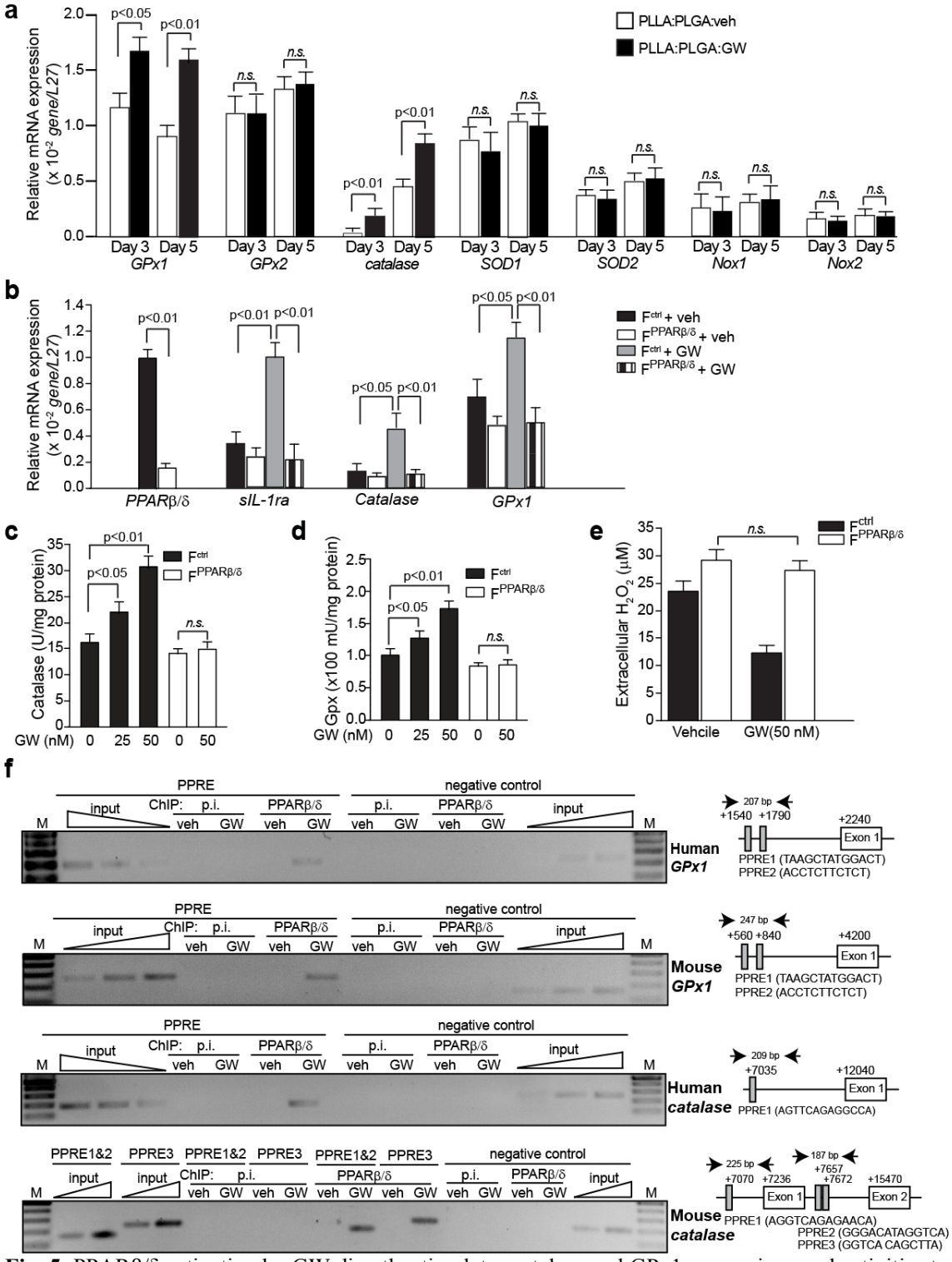

Fig. 5. PPARβ/δ activation by GW directly stimulates catalase and GPx1 expressions and activities to diminish fibroblast H_2O_2 production. (a) Relative mRNA expression of various ROS-related genes in wound fibroblasts extracted by LCM from PLLA:PLGA:veh- or PLLA:PLGA:GW-treated wound biopsies at indicated time points. (b) Relative mRNA expression of various genes and (c-e) Catalase (c) and GPx (d) activities, and (e) extracellular H_2O_2 levels on *in vitro* cultured fibroblast or its PPARβ/δ counterpart upon indicated treatments. Data (mean ± SD), n ≥ 4. (f) Results of ChIP assay conducted using pre-immune IgG (p.i.) or antibody against PPARβ/δ in vehicle (veh) or GW treated

fibroblasts. Specific regions (PPREs, respective sequences shown at the right panels) spanning promoter binding sites of the *GPx1* and *catalase* genes (from both human and mouse origins) were amplified using appropriate primers (Table S1). A control region served as a negative control.

4. Discussion

Numerous studies have been conducted to develop more efficient systems of drug delivery for wound healing. However, much remain to learn about how the efficacy of a potential drug on diabetic wound healing may be affected by different drug release kinetics. In the present study, we introduced single-layered PLLA:GW, PLGA:GW and double-layered PLLA:PLGA:GW microparticles as potential formulations for an efficient wound healing. The rationale behind the use of PLLA, PLGA and PLLA:PLGA is to deliver the encapsulated hydrophobic PPARβ/δ ligand GW501516 (GW) topically with delayed and early release profiles, respectively and at the same time examine the therapeutic potential of GW on the healing rate of full-thickness excisional splint wounds of diabetic mice.

We have prepared PLLA:GW, PLGA:GW and PLLA:PLGA:GW by using the oil-in-water emulsion solvent evaporation technique that resulted in spherical microparticles of size ranging from 75-125 μm with high GW encapsulation. There are differences in average drug loading between microparticle formulations (PLLA:GW 0.065%, PLGA:GW 0.07% versus PLLA:PLGA:GW 0.2%). The encapsulation efficiency of PLLA:PLGA:GW particles was higher than that of PLLA and PLGA microparticles, possibility to the fact that PLGA helped to shield the drug disperse into PLLA from outer aqueous phase during fabrication**.** The PLLA:GW, PLGA:GW and PLLA:PLGA:GW retained the biological activity, enhanced the *in vivo* bio-stability and overcame the hydrophobicity problem of GW for topical application. This mode of delivery was adopted for drug administration to reduce the compounding systemic influences of GW and potential off-target side effects. The three formulations of encapsulation provided two distinctive release kinetics of GW. *In vitro* drug release of double-layered PLLA:PLGA:GW showed a rapid initial release followed by a gradual and sustained drug release. In contrast, the release of GW from PLLA:GW and PLGA:GW was initially slow, followed by a drastic increase to its peak by day 10. Moreover, the increased expression of PPARβ/δ target genes in fibroblasts and keratinocytes, two major cell types that constitutes the skin, confirmed that the preparation technique neither destroyed nor modified GW and its biological activity.

The physiological impact of non-encapsulated GW, PLLA:GW, PLGA:GW and PLLA:PLGA:GW on wound healing were evaluated in a splinted diabetic mouse full thickness excisional model. PPARβ/δ plays multiple roles in wound healing, such as angiogenesis, and keratinocytes viability and migration [18, 30, 33, 34]. Indeed, we found that PPARβ/δ agonist GW accelerates diabetic wound closure. Interestingly, the drug release profile has a dramatic effect on the efficacy in wound healing. GW was released from PLLA:PLGA:GW in the early phase and remain sustained throughout the rest of the healing process. In contrast, GW was only released from PLLA:GW and PLGA:GW during the later stages of wound repair.

Diabetic wounds are characterised by an early excessive and protracted ROS production, which coincides with an aberrant inflammatory response [35]. Such dysregulated ROS level impairs multiple cellular processes and responsiveness to external signals, leading to delayed wound healing [36, 37]. Consistent with previous reports, we found an excessive H_2O_2 level in the diabetic wound microenvironment. We also revealed that fibroblasts and macrophages were major contributors of this oxidative microenvironment. Collagen, the major matrix protein in the wound bed, was modified by H_2O_2 at several amide positions. Furthermore, the migration of keratinocyte was impaired on this modified matrix. An early

release of GW resulted in increased expressions and activities of GPx1 and catalase, which would facilitate the conversion of H_2O_2 to H_2O, consequently reining the oxidative modifications of ECM. The increased expressions of these two genes were mediated by ligand activation of PPARβ/δ. This was evidenced by the elevated levels of intracellular and extracellular H_2O_2 in the presence of PPARβ/δ antagonists GSK and Cpd, the inability of GW to quench extracellular H_2O_2 when PPARβ/δ was knocked-down in fibroblasts, the identification of a functional PPRE in the promoter of these two genes and our subsequent ChIP experiment in the presence of GW. As such, an earlier and timely release of GW dosage to the diabetic wound reduced accumulation of ROS, in particular H_2O_2 in the diabetic wounds, via the continuous activation of GPx1 and catalase. Conceivably, a delayed release of GW, as in the case of PLLA:GW and PLGA:GW, would not be able to prevent this modification of the ECM during the early stages of wound repair, thereby retarding the migration of keratinocytes in the subsequent stage of wound closure.

The microencapsulation of GW in our study to target diabetic wounds underscored the importance of drug release kinetics on the outcome of a treatment. Microparticles to deliver GW to the diabetic wounds in a controlled release manner allowed us to understand how the release kinetics of a single drug from different microparticles can have different healing outcomes. Importantly, it provided novel insights into the roles of PPARβ/δ in wound healing which would not have been possible if GW had been directly applied topically. Presumably, direct topical application, without any sustained release, may affect the early stages of wound healing, but subsequently has a diminished impact on the rest of the cellular events, such as angiogenesis and keratinocyte migration. Wound healing rate was faster in non-encapsulated GW-treated wounds when compared to vehicle treatment. The healing rate was transiently slower when compared to wounds treated with single-layered microencapsulated GW, which may be due to the resultant effects from the stability, bioavailability and cytotoxicity by a single large bolus exposure to GW which could be difficult to predict *in vivo*. Further such variations would likely diminish the pharmaceutical use of GW as a wound healing drug. Therefore, microencapsulation of GW to allow for controlled drug release empowers us to better appreciate the therapeutic potential of GW as a wound healing drug.

Our study herein has demonstrated the importance of being able to deliver a drug to its target in a controlled release manner. Besides having better patient compliance, the use of such carriers can allow for reduced drug quantity having the same desired therapeutic effects in patients. We have also established that different release kinetics could result in different efficacies of a particular drug. Importantly, the encapsulation of the drug is able to maintain the integrity of the drug, as well as, improving drug delivery efficacy by overcoming problems rendered by the hydrophobic nature and stability of GW. Thus, PLLA:PLGA:GW serves as an important starting tool towards further development of more affordable and effective clinical therapies for diabetic wound healing.

5. Conclusions

In this study, the efficacies of PPARβ/δ agonist GW-loaded microparticles on diabetic wound healing were investigated through topical application. We showed that microparticles, PLLA:GW, PLGA:GW and PLLA:PLGA:GW, accelerated diabetic wound closure, albeit with different release kinetics and efficacies. PLLA:PLGA:GW has an earlier controlled release of GW and significant improvement on the wound healing when compared with PLLA:GW and PLGA:GW. Our study also revealed a novel protective role of PPARβ/δ on ECM against the detrimental ROS. We identified two novel PPARβ/δ target genes *GPx1* and *catalase*, their elevated expression scavenged excessive H_2O_2 in diabetic wounds, minimized H_2O_2-induced ECM modifications, restored keratinocyte migration and therefore diabetic wound healing. The present study underscores the important relationship between controlled

drug release kinetics and therapeutic efficacy. Therefore more investigations are warranted to better appreciate the full potential of controlled drug release.

Acknowledgement

We thank the National Medical Research Council, Singapore (NMRC/1280/2010) for supporting this research. MKS is a recipient of the Research Scholarship of the Nanyang Technological University, Singapore. We thank Mr. Twang Jing Shun for his input on the graphical abstract.
Author contributions: XW, MKS and SF designed and performed the experiments, analysed the data with intellectual inputs from PZ and NST. HCC, PZ and MBYT performed some studies and provided technical help. WLL, KWN and SCJL prepared and characterized the microparticles. BMKT and SC synthesized agonists and antagonists. MTCW provided the adult human skin tissues. MKS, PZ and NST were involved in manuscript preparation.

References

[1] S. Wild, G. Roglic, A. Green, R. Sicree, H. King. Global prevalence of diabetes: estimates for the year 2000 and projections for 2030. Diabetes Care 27 (2004) 1047-1053.

[2] P. Palumbo, L. Melton, C. Haskell. Peripheral vascular disease and diabetes. Diabetes in America p 85 (1985) XV1-XV20.

[3] R.E. Pecoraro, G.E. Reiber, E.M. Burgess. Pathways to diabetic limb amputation. Basis for prevention. Diabetes Care 13 (1990) 513-521.

[4] H. Brem, M. Tomic-Canic. Cellular and molecular basis of wound healing in diabetes. J Clin Invest 117 (2007) 1219-1222.

[5] T. Velnar, T. Bailey, V. Smrkolj. The wound healing process: an overview of the cellular and molecular mechanisms. J Int Med Res 37 (2009) 1528-1542.

[6] S. Schreml, M. Landthaler, M. Schäferling, P. Babilas. A new star on the H□O□rizon of wound healing? Exp Dermatol 20 (2011) 229-231.

[7] S. Roy, S. Khanna, K. Nallu, T.K. Hunt, C.K. Sen. Dermal wound healing is subject to redox control. Mol Ther 13 (2006) 211-220.

[8] C.K. Sen. The general case for redox control of wound repair. Wound Repair Regen 11 (2003) 431-438.

[9] N. Bryan, H. Ahswin, N. Smart, Y. Bayon, S. Wohlert, J.A. Hunt. Reactive oxygen species (ROS)--a family of fate deciding molecules pivotal in constructive inflammation and wound healing. Eur Cell Mater 24 (2012) 249-265.

[10] U. auf dem Keller, A. Kümin, S. Braun, S. Werner. Reactive oxygen species and their detoxification in healing skin wounds. J Investig Dermatol Symp Proc 11 (2006) 106-111.

[11] M. Mizuta, S. Hirano, S. Ohno, I. Tateya, S.I. Kanemaru, T. Nakamura, J. Ito. Expression of reactive oxygen species during wound healing of vocal folds in a rat model. Ann Otol Rhinol Laryngol 121 (2012) 804-810.

[12] A.M. Rasik, A. Shukla. Antioxidant status in delayed healing type of wounds. Int J Exp Pathol 81 (2000) 257-263.

[13] N.S. Tan, G. Icre, A. Montagner, B. Bordier-ten-Heggeler, W. Wahli, L. Michalik. The nuclear hormone receptor peroxisome proliferator-activated receptor beta/delta potentiates cell chemotactism, polarization, and migration. Mol Cell Biol 27 (2007) 7161-7175.

[14] N.S. Tan, L. Michalik, N. Di-Poï, C.Y. Ng, N. Mermod, A.B. Roberts, B. Desvergne, W. Wahli. Essential role of Smad3 in the inhibition of inflammation-induced PPARbeta/delta expression. EMBO J 23 (2004) 4211-4221.

[15] N. Di-Poi, N. Tan, L. Michalik, W. Wahli, B. Desvergne. Antiapoptotic role of PPARbeta in keratinocytes via transcriptional control of the Akt1 signaling pathway. Mol Cell 10 (2002) 721-733.

[16] H.C. Chong, J.S.K. Chan, C.Q. Goh, N.V. Gounko, B. Luo, X. Wang, S. Foo, M.T.C. Wong, C. Choong, S. Kersten, N.S. Tan. Angiopoietin-like 4 stimulates STAT3-mediated iNOS expression and enhances angiogenesis to accelerate wound healing in diabetic mice. Mol Ther 22 (2014) 1593-1604.

[17] H.C. Chong, M.J. Tan, V. Philippe, S.H. Tan, C.K. Tan, C.W. Ku, Y.Y. Goh, W. Wahli, L. Michalik, N.S. Tan. Regulation of epithelial-mesenchymal IL-1 signaling by PPARbeta/delta is essential for skin homeostasis and wound healing. J Cell Biol 184 (2009) 817-831.

[18] N.S. Tan, L. Michalik, B. Desvergne, W. Wahli. Genetic- or transforming growth factor-beta 1-induced changes in epidermal peroxisome proliferator-activated receptor beta/delta expression dictate wound repair kinetics. J Biol Chem 280 (2005) 18163-18170.

[19] L. Michalik, W. Wahli. Involvement of PPAR nuclear receptors in tissue injury and wound repair. J Clin Invest 116 (2006) 598-606.

[20] E. Wenk, A.J. Meinel, S. Wildy, H.P. Merkle, L. Meinel. Microporous silk fibroin scaffolds embedding PLGA microparticles for controlled growth factor delivery in tissue engineering. Biomaterials 30 (2009) 2571-2581.
[21] G. Gainza, J.J. Aguirre, J.L. Pedraz, R.M. Hernández, M. Igartua. rhEGF-loaded PLGA-Alginate microspheres enhance the healing of full-thickness excisional wounds in diabetised Wistar rats. Eur J Pharm Sci 50 (2013) 243-252.
[22] S. Huang, T. Deng, Y. Wang, Z. Deng, L. He, S. Liu, J. Yang, Y. Jin. Multifunctional implantable particles for skin tissue regeneration: preparation, characterization, in vitro and in vivo studies. Acta Biomater 4 (2008) 1057-1066.
[23] X. Dong, J. Xu, W. Wang, H. Luo, X. Liang, L. Zhang, H. Wang, P. Wang, J. Chang. Repair effect of diabetic ulcers with recombinant human epidermal growth factor loaded by sustained-release microspheres. Sci China C Life Sci 51 (2008) 1039-1044.
[24] H.K. Makadia, S.J. Siegel. Poly Lactic-co-Glycolic Acid (PLGA) as Biodegradable Controlled Drug Delivery Carrier. Polymers 3 (2011) 1377-1397.
[25] W.L. Lee, M. Hong, E. Widjaja, S.C.J. Loo. Formation and degradation of biodegradable triple-layered microparticles. Macromolecular rapid communications 31 (2010) 1193-1200.
[26] W.L. Lee, W.L. Foo, E. Widjaja, S.C.J. Loo. Manipulation of process parameters to achieve different ternary phase microparticle configurations. Acta Biomater 6 (2010) 1342-1352.
[27] W.L. Lee, Y.C. Seh, E. Widjaja, H.C. Chong, N.S. Tan, S.C.J. Loo. Fabrication and drug release study of double-layered microparticles of various sizes. J Pharm Sci 101 (2012) 2787-2797.
[28] N. Tan, W. Wahli. Studying Wound Repair in the Mouse. Curr. Protoc. Mouse Biol. 3 (2013) 171-185.
[29] M. Pal, M.J. Tan, R.L. Huang, Y.Y. Goh, X.L. Wang, M.B.Y. Tang, N.S. Tan. Angiopoietin-like 4 regulates epidermal differentiation. PloS one 6 (2011) e25377.
[30] H. Chong, J. Chan, C. Goh, N. Gounko, B. Luo, X. Wang, S. Foo, M. Wong, C. Choong, S. Kersten, N. Tan. ANGPTL4 stimulates STAT3-mediated iNOS expression and enhances angiogenesis to accelerate wound healing in diabetic mice. Mol Ther 22 (2014) 1593-1604.
[31] B.G. Shearer, D.J. Steger, J.M. Way, T.B. Stanley, D.C. Lobe, D.A. Grillot, M.A. Iannone, M.A. Lazar, T.M. Willson, A.N. Billin. Identification and characterization of a selective peroxisome proliferator-activated receptor beta/delta (NR1C2) antagonist. Mol Endocrinol 22 (2008) 523-529.
[32] S. Naruhn, P.M. Toth, T. Adhikary, K. Kaddatz, V. Pape, S. Dörr, G. Klebe, S. Müller-Brüsselbach, W.E. Diederich, R. Müller. High-affinity peroxisome proliferator-activated receptor β/δ-specific ligands with pure antagonistic or inverse agonistic properties. Mol Pharmacol 80 (2011) 828-838.
[33] N.S. Tan, L. Michalik, N. Di-Poï, B. Desvergne, W. Wahli. Critical roles of the nuclear receptor PPARbeta (peroxisome-proliferator-activated receptor beta) in skin wound healing. Biochem Soc Trans 32 (2004) 97-102.
[34] N.S. Tan, L. Michalik, N. Noy, R. Yasmin, C. Pacot, M. Heim, B. Flühmann, B. Desvergne, W. Wahli. Critical roles of PPAR beta/delta in keratinocyte response to inflammation. Genes Dev 15 (2001) 3263-3277.
[35] E. Aktunc, V.H. Ozacmak, H.S. Ozacmak, F. Barut, M. Buyukates, O. Kandemir, N. Demircan. N-acetyl cysteine promotes angiogenesis and clearance of free oxygen radicals, thus improving wound healing in an alloxan-induced diabetic mouse model of incisional wound. Clin Exp Dermatol 35 (2010) 902-909.

[36] M. De Mattei, A. Ongaro, S. Magaldi, D. Gemmati, A. Legnaro, A. Palazzo, F. Masieri, A. Pellati, L. Catozzi, A. Caruso, P. Zamboni. Time- and dose-dependent effects of chronic wound fluid on human adult dermal fibroblasts. Dermatol Surg 34 (2008) 347-356.
[37] S.A. Eming, T. Krieg, J.M. Davidson. Inflammation in wound repair: molecular and cellular mechanisms. J Invest Dermatol 127 (2007) 514-525.

Early controlled release of peroxisome proliferator-activated receptor β/δ agonist GW501516 improves diabetic wound healing through redox modulation of wound microenvironment.

Xiaoling WANG[1#], Ming Keat SNG[1#], Selin FOO[1], Han Chung CHONG[1], Wei Li LEE[2], Mark Boon Yang TANG[3], Kee Woei NG[2], Baiwen LUO[2], Cleo CHOONG[2], Marcus Thien Chong WONG[4], Benny Meng Kiat TONG[5], Shunsuke CHIBA[5], Say Chye Joachim LOO[2], Pengcheng ZHU[1*], Nguan Soon TAN[1,6*]

[1]School of Biological Sciences, Nanyang Technological University, 60 Nanyang Drive, Singapore 637551.
[2]School of Materials Science and Engineering, Nanyang Technological University, Singapore 639798.
[3]National Skin Centre, 1 Mandalay Road, Singapore 308205.
[4]Tan Tock Seng Hospital, 11 Jalan Tan Tock Seng, Singapore 308433.
[5]Division of Chemistry and Biological Chemistry, School of Physical and Mathematical Sciences, Nanyang Technological University, 21 Nanyang Link, Singapore 637371.
[6]Institute of Molecular and Cell Biology, 61 Biopolis Drive, Proteos, Singapore 138673.

[#]Authors contributed equally

*Co-corresponding authors:
PZ: pczhu@ntu.edu.sg
NST: nstan@ntu.edu.sg or nstan@imcb.a-star.edu.sg; Tel: +65-6316-2941; Fax: +65-67913856

Supplementary Information

Supplementary material and methods

Cell culture.

Human keratinocytes (Cascade Biologics) were routinely cultured in Keratinocyte-SFM (Invitrogen). Adult human dermal fibroblasts were isolated by explant method from human abdominal skins as previously described [1]. Human abdominal skins tissue were provided by Dr. Marcus Wong from Plastic, Reconstructive and Aesthetic Surgery of Tan Tock Seng Hospital Singapore under an ethical committee review board approval with reference number (NHG DSRB Ref: 2012/00071). The adult wound fibroblasts were routinely cultured in FibroGRO complete media (Millipore). Immortalized human keratinocyte HaCaT and human embryonic kidney (HEK 293T) cells were maintained in DMEM supplemented with 10% fetal bovine serum (FBS). Human monocyte THP-1 was cultured in RPMI-1640 medium supplemented with 10% FBS. Differentiation of THP-1 to macrophages is triggered by addition of PMA (50 ng/ml) and overnight incubation. Diabetic condition was achieved as previously described [2]. All cell lines were maintained in a humidified incubator at 37 ^{o}C with 5 % CO_2.

Histology study.

Wound biopsies were sectioned for immunohistochemistry as described [3]. Briefly, tissue specimens were fixed with 4% paraformaldehyde, dehydrated and embedded in paraffin according to standard procedure. 5 µm-thick paraffin tissue sections were cut using Leica RM2235 rotary microtome (Leica Biosystems) and mounted on SuperFrost Plus slides (Thermo Fisher Scientific). The sections were then deparaffinized and rehydrated for staining analyses. Standard haematoxylin & eosin (H&E) staining was performed.

Laser capture microdissection (LCM).

H&E stained wound sections were subjected to LCM using Arcturus® XT laser capture microdissection system according to the manufacturer's instructions (Life technologies). LCM tissues (dermal fibroblasts) were collected onto an adhesive CapSure® Macro LCM Caps (Life technologies). Samples were capped onto 500 ml centrifuging tubes containing 15 µl of lysis buffer and processed for RNA extraction and qPCR analysis.

Reverse transcription polymerase chain reaction (RT-PCR) and real-time quantitative PCR (qPCR).

Samples (cultured cell pellets or skin wound tissues) were homogenized in TRIzol (Invitrogen Life Technologies) and total RNA was purified following the manufacturer's instructions. Reverse transcription was performed using *iScrpt™ cDNA* Synthesis kit (Bio-Rad). qPCR was performed using SYBR Green PCR Master Mix (Applied Biosystem, CA) in a *CFX96* Touch real-time *PCR* detection system. Sequences of the gene-specific primers are shown as follows.

Genes	Forward (5' to 3')	Reverse (5' to 3')
Gpx1	AATGTCGCGTCTCTCTGAGG	TCCGAACTGATTGCACGGG
Gpx2	GAGCTGCAATGTCGCTTTCC	TGGGTAAGACTAAAGGTGGGC
SOD1	ATGGCGATGAAAGCGGTGT	CCTTGTGTATTGTCCCCATACTG
catalase	CCCCTATTGCCGTTCGATTCT	TTCAGGTGAGTCTGTGGGTTT
sIL-1ra	CTCAGATAGAAGGTCTTCTGG	CCGCAGTCACCTAATCACTCTCCT
Nox1	CTGCTTCCTGTGTGTCGCAA	AGGCAGATCATATAGGCCACC
Nox2	GAAGAAAGGCAAACACAACACA	CCCCAGCCAAACCAGAAT
ANGPTL4	CCTCATGGTCTAGGTGCTTGT	GTCCACCGACCTCCCGTTA
L27	AATGCCCACAAGGTACTCTGT	CTTGCGTTTAAGAGCAGGATCT

Chromatin immunoprecipitation (ChIP) assay.

ChIP was performed as described previously with minor modifications [4]. Briefly, fibroblasts with respective treatments were collected and cross-linked using 1% formaldehyde for 15 min at 37 ^{o}C prior to sonication in in lysis buffer. Monoclonal anti-PPARβ/δ (Millipore) antibody was used. The immunoprecipitates were reverse cross-linked for PCR by heating at 65 ^{o}C for 6 h. The primer pairs used are shown in the follow table.

Oligo name	Forward (5' to 3')	Reverse (5' to 3')
hcatalasePPRE1	TCCAAGCATGTGAATCCCAGTAG	CTGAGTCCTACTCAAGCCATCTCC
hGpx1PPRE1,2	GGTCCAGGTTACCCTTCCAAG	GAGGGATCTAGGCTTCCGGT
mcatalasePPRE1	ACCACCCACAAATTAGTAGCAAACAAAG	GATAGGAAGAGACTGGGGA
mcatalasePPRE2,3	ACCCACAAATTAGTAGCAAACAAAG	CCAATCCCGTCCTTTCTAGAGT
mGpx1PPRE1,2	TACCTGACCTGTTGCTCCCTT	AACTACTGTGTCTATTAAACTT

Supplementary figures and tables

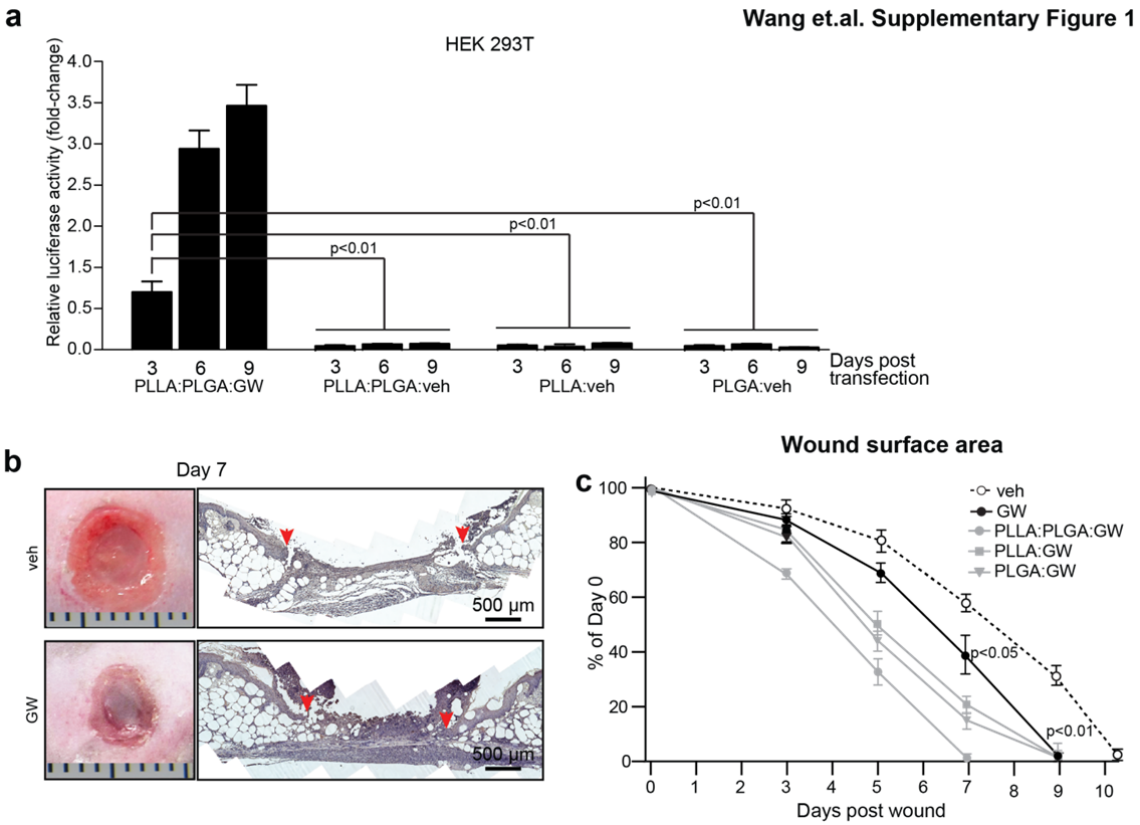

Sup. Fig. 1. Properties of vehicle encapsulated microparticles and therapy effects of GW (dissolved in DMSO) on diabetic wound. (a) Drug release kinetics of microparticles measured in HEK 293T. Relative luciferase activities were normalized to Renilla luciferase activities. (b) Representative macroscopic wounds (left) and H&E (right) sections of diabetic wounds from indicated test groups (n = 5) at day 7. Ruler units are in mm. Red arrows point to epithelial wound edge. (c) Wounds closure kinetics of mice treated with indicated GW and vehicle. Data points and curves in grey color are retrieved from Fig. 2b and re-plotted here for comparison. Wound surface area are plotted as percentage of day 0 (=100%).

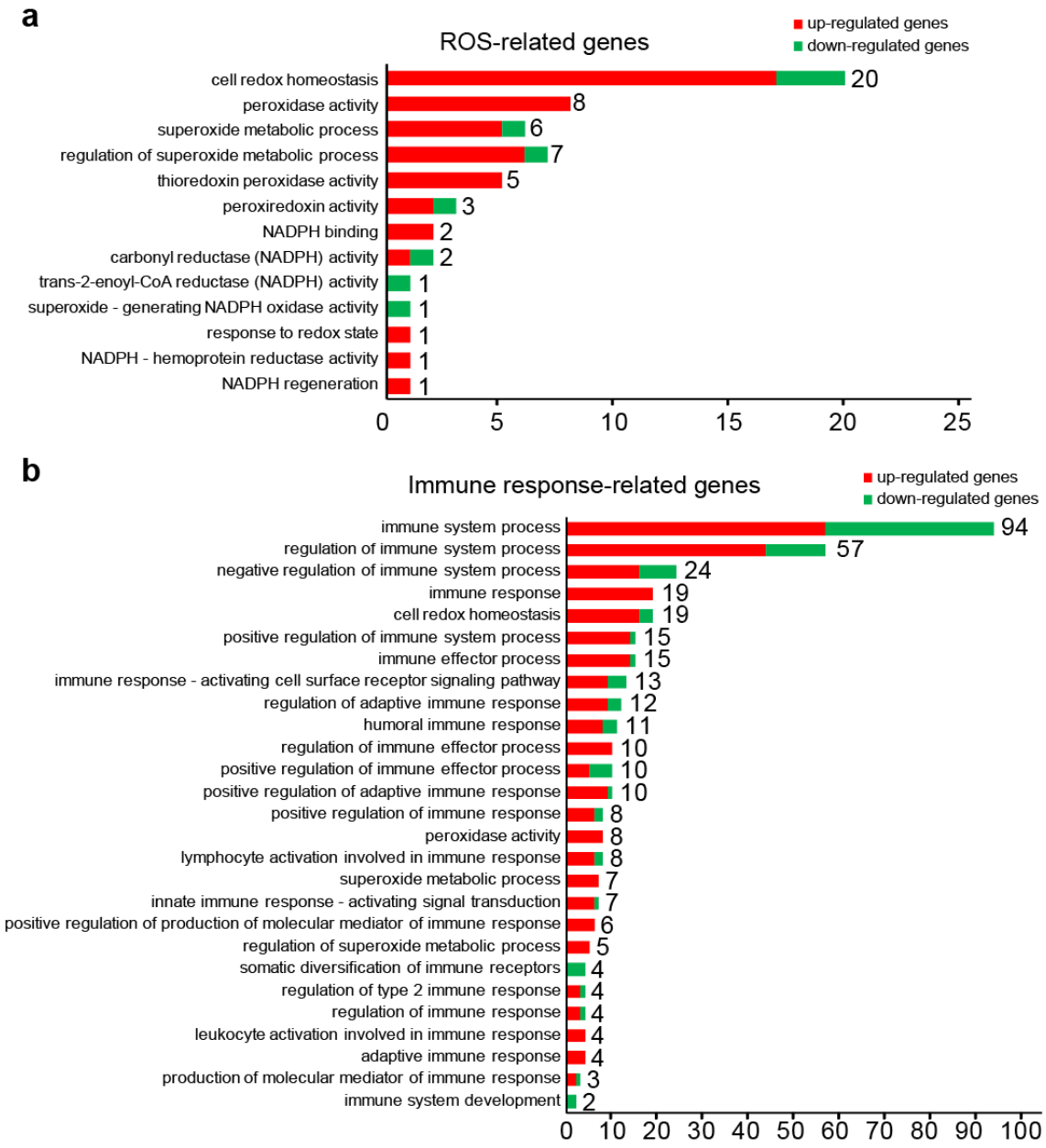

Sup. Fig. 2. Gene ontology analysis comparing PLLA:PLGA:GW- and PLLA:PLGA:veh-treated wounds. Graphs showed the expression of (a) ROS-related genes and (b) Immune response-related genes from gene expression microarray. Numbers beside the bar indicate number of genes. The gene list and fold change are in Tables S1 and S2.

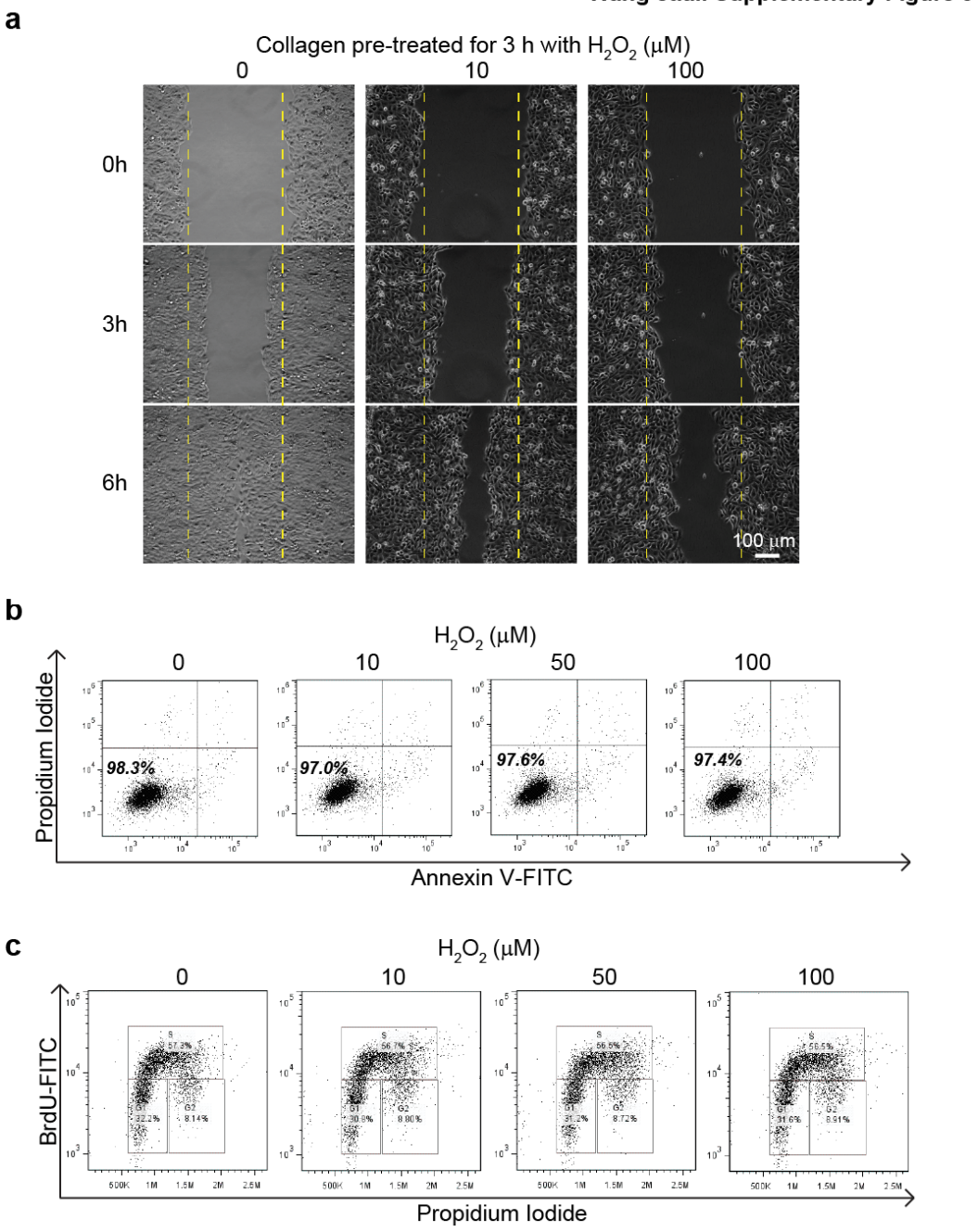

Sup. Fig. 3. H_2O_2 modifies collagen to hamper keratinocyte migration. (a) Representative time-lapsed images of scratch wounded cultures of keratinocytes. Culture plates were pre-coated with type I collagen and treated with or without indicated concentrations of H_2O_2 for 3 h before being used for the wound assay. Yellow dotted lines represent the wound gap at the time of wounding. Scale bars 100 μm. (b) FACS graphs on Annexin V (AV) and propidium iodide (PI) staining assays done on keratinocytes with indicated treatments. As analyzed by FACS (5000 events), the sum of Annexin V-/PI- cells were considered healthy. Values (bold) denote survival cells (%). (c) FACS graphs on cell cycle analysis using BrdU staining keratinocytes with indicated treatments. Percentage of various cell cycle phases as segregated within different rectangles. Results are representative of three independent experiments performed three or four times with consistent results.

Table S1. Expression of ROS related genes.

Gene Symbol	Gene ID	Fold Change of PLLA:PLGA:GW- vs. PLLA:PLGA:veh-treated biopsies		Gene Ontology Function
		Day 3	Day 5	
Cbr2	NM_007621	2.05862	1.31167	carbonyl reductase (NADPH) activity
Cbr3	NM_173047	-1.6893	-1.18594	
Dnajc10	NM_024181	7.5363	1.72642	cell redox homeostasis
Magt1	NM_001190409	6.05322	1.73061	
Aifm1	NM_012019	6.04561	1.36081	
Txn1	NM_011660	5.86263	1.17753	
Krit1	NR_033173	5.21196	1.25766	
P4hb	NM_011032	4.81143	2.04824	
Txndc9	NM_172054	4.2407	1.22302	
2810407C02Rik	NM_001040396	3.18237	1.41236	
Dld	NM_007861	2.5581	1.24805	
Glrx	NM_053108	2.48584	1.79347	
Tmx1	NM_028339	2.46694	1.62976	
Il6	NM_031168	2.2372	2.65185	
Sh3bgrl3	ENSMUST00000030651	2.14773	1.23318	
Qsox1	NM_001024945	1.8022	1.37962	
Pdia4	NM_009787	1.72525	1.03597	
Gsr	NM_010344	1.60079	2.01883	
Tusc3	NM_030254	1.23176	1.51385	
Glrx3	NM_023140	-1.58038	-1.79953	
Txndc8	NM_026132	-1.72146	-1.30604	
Grxcr1	NM_001018019	-2.0417	-1.07777	
Cbr4	NM_145595	4.57129	1.92942	NADPH binding
Decr1	NM_026172	2.77655	1.01894	
Pgd	NM_001081274	2.22418	1.0421	NADPH regeneration
Por	NM_008898	1.73584	1.43756	NADPH-hemoprotein reductase activity
Mgst1	NM_019946	5.9749	1.3022	peroxidase activity
Gpx8	NM_027127	5.46632	1.14281	
Cat	NM_009804	3.4342	2.02084	
Alox5ap	NM_009663	2.01433	3.36222	
Pxdn	NM_181395	1.76767	1.20692	
Mgst3	NM_025569	1.51937	1.07872	
Ptgs1	NM_008969	1.50134	1.33969	
Gpx1	NM_008160	2.12751	1. 42129	
Prdx4	NM_016764	2.24803	1.64112	peroxiredoxin activity
Prdx6	NM_007453	2.23773	1.01909	
Prdx5	ENSMUST00000025904	-1.04655	1.55561	

Nfe2l2	NM_010902	13.4134	2.91583	regulation of superoxide metabolic process
Cd36	NM_001159557	9.14596	1.16784	
Il18	NM_008360	4.079	1.80827	
Egfr	NM_207655	2.33444	1.29242	
Aatf	NM_019816	1.81948	1.50574	
Agtr1a	NM_177322	1.57849	1.04589	
F2rl1	NM_007974	-1.7646	-1.7244	
Adh5	NM_007410	2.37215	1.29995	response to redox state
Cybb	NM_007807	5.34756	8.18011	superoxide metabolic process
Sh3pxd2a	NM_008018	4.97967	1.72867	
Cyb5r4	NM_024195	3.93283	1.82945	
Cyb5r4	NM_024195	3.57342	2.09008	
Atp7a	NM_001109757	1.82968	1.56075	
Edn1	NM_010104	-1.15968	1.50728	
Ncf2	NM_010877	-2.89628	-1.37019	superoxide-generating NADPH oxidase activity
Prdx1	NM_011034	4.49224	2.27324	thioredoxin peroxidase activity
Sep-15	NM_053102	3.88999	1.11073	
Prdx2	NM_011563	3.55543	1.48208	
Prdx1	NM_011034	3.2337	2.45724	
Prdx2	ENSMUST00000109734	2.55969	3.38465	
Pecr	NM_023523	-1.86497	-1.16975	trans-2-enoyl-CoA reductase (NADPH) activity

Table S2. Expression of immune response-related genes.

Gene Symbol	Gene ID	Fold Change of PLLA:PLGA:GW- vs. PLLA:PLGA:veh-treated biopsies		Gene Ontology Function
		Day 3	Day 5	
Nedd4	NM_010890	4.30301	1.70627	adaptive immune response
Ctsh	NM_007801	3.87012	1.96373	
Lilrb3	NM_011095	3.62063	2.01852	
Adam17	NM_009615	2.42499	2.28553	
Dnajc10	NM_024181	7.5363	1.72642	cell redox homeostasis
Magt1	NM_001190409	6.05322	1.73061	
Aifm1	NM_012019	6.04561	1.36081	
Txn1	NM_011660	5.86263	1.17753	
Krit1	NR_033173	5.21196	1.25766	
P4hb	NM_011032	4.81143	2.04824	
Txndc9	NM_172054	4.2407	1.22302	
2810407C02Rik	NM_001040396	3.18237	1.41236	
Dld	NM_007861	2.5581	1.24805	
Glrx	NM_053108	2.48584	1.79347	
Tmx1	NM_028339	2.46694	1.62976	
Sh3bgrl3	ENSMUST00000030651	2.14773	1.23318	
Qsox1	NM_001024945	1.8022	1.37962	
Pdia4	NM_009787	1.72525	1.03597	
Gsr	NM_010344	1.60079	2.01883	
Tusc3	NM_030254	1.23176	1.51385	
Glrx3	NM_023140	-1.58038	-1.79953	
Txndc8	NM_026132	-1.72146	-1.30604	
Grxcr1	NM_001018019	-2.0417	-1.07777	
Cfh	NM_009888	12.574	2.01242	humoral immune response
Cfb	NM_008198	5.66608	4.87115	
Serping1	NM_009776	4.82581	3.59873	
Cfp	NM_008823	2.02194	1.74565	
C1qb	NM_009777	1.69917	1.8	
Rbpj	NM_009035	1.67255	1.81147	
C1s	NM_144938	1.64529	1.71535	
Bmi1	NM_007552	1.58656	1.81977	
Cr1l	NM_013499	-1.03976	-1.60131	
C8g	NM_027062	-1.70627	1.51436	
Ighm	BC053409	-1.69679	-1.62015	
Rnasel	NM_011882	15.5147	2.11269	immune effector process
Bnip3l	NM_009761	7.2296	3.31257	
Ifitm1	NM_026820	2.8797	1.52035	

Mll5	NM_026984	2.68176	1.65866	
Apobec1	NM_031159	2.17579	1.60903	
Ifitm3	NM_025378	2.02428	3.38953	
Eif2ak2	NM_011163	1.96352	2.04967	
Ifit3	NM_010501	1.91434	2.9002	
Ptx3	NM_008987	1.61419	2.23212	
Ifnar1	NM_010508	1.56055	1.90855	
Ifna2	NM_010503	1.53718	2.27848	
Oas2	NM_145227	1.38925	1.81569	
Ifitm2	NM_030694	1.08772	1.9322	
Gm13280	NM_206867	1.0143	3.02008	
Fut7	NM_013524	-1.23835	-1.66168	
Prg4	NM_021400	34.1871	1.54689	immune response
Ly96	NM_016923	17.6354	2.1893	
Ccl11	NM_011330	13.2333	1.76715	
Clec4e	NM_019948	4.75147	4.33999	
Enpp1	NM_008813	4.6931	1.57095	
Ccl6	NM_009139	4.25482	2.0765	
Ccl12	NM_011331	3.44691	1.88498	
Ccl9	NM_011338	3.40896	2.37272	
Lcn2	NM_008491	2.17977	5.95566	
Clec4a2	NM_001170333	2.15729	3.03311	
Clec4d	NM_010819	1.97196	2.7971	
Pf4	NM_019932	1.67868	3.10926	
Cxcl3	NM_203320	1.57223	3.68233	
Clec4n	NM_020001	1.50471	4.13891	
Csf1r	NM_001037859	1.46636	2.59322	
Ly86	NM_010745	1.36699	1.51563	
Naip2	NM_010872	1.07172	1.68188	
Naip5	NM_010870	1.04724	1.64674	
Hck	NM_010407	1.03704	1.55535	
Ube2n	NM_080560	7.59293	1.45007	immune response-activating cell surface receptor signaling pathway
Cd38	NM_007646	7.38302	6.42686	
Ube2n	NM_080560	7.36737	1.45427	
C3ar1	NM_009779	4.27815	6.63313	
Nckap1l	NM_153505	4.04978	2.27033	
Ptpn22	NM_008979	2.39281	1.08358	
Mapk1	NM_011949	1.72754	1.14953	
Plcg1	NM_021280	1.59743	1.09029	
Prkcb	NM_008855	1.5968	1.00956	
Lime1	NM_023684	-1.02061	-1.53681	
Cd19	NM_009844	-1.11141	-2.0396	
Gpld1	NM_008156	-1.3384	-1.76269	
Itk	NM_010583	-2.17581	-1.26318	

Spef2	NM_177123	-2.12649	-1.23153	immune system development
Spef2	HQ856050	-2.15837	-2.94716	
Ddx3x	NM_010028	19.7938	1.0257	immune system process
Spp1	NM_001204233	16.0907	1.72213	
Bnip3	NM_009760	15.2109	1.14843	
Fyb	ENSMUST00000090461	9.13032	7.69649	
Rps24	NM_011297	8.82003	1.51365	
Hprt	NM_013556	7.88289	1.5558	
Skap2	NM_018773	7.53205	1.61556	
Cd48	ENSMUST00000068584	6.60732	2.36939	
Rock1	ENSMUST00000067947	5.41465	1.21859	
Wwp1	NM_177327	4.85088	1.4686	
Rps24	NM_011297	4.83852	1.19876	
Jak2	NM_008413	4.63477	1.04391	
Dicer1	NM_148948	4.49698	1.40007	
Rac1	ENSMUST00000080537	4.10445	2.02798	
Ctsc	NM_009982	3.8931	1.325	
Chd7	NM_001081417	3.6337	1.80133	
Cd34	NM_001111059	3.47439	2.32254	
Herc6	NM_025992	3.16515	1.29776	
Iigp1	NM_001146275	3.16247	1.773	
Tshr	NM_011648	3.04609	1.08505	
Gon4l	NM_001242372	2.91174	1.02861	
Itgam	NM_001082960	2.86228	2.28844	
Abcc9	ENSMUST00000073173	2.80884	1.45056	
Rps17	NM_009092	2.78681	1.81688	
Ifitm1	NM_001112715	2.61809	1.15712	
Cxcr2	NM_009909	2.56447	1.8194	
Cxcl16	NM_023158	2.53035	1.48077	
Psme1	NM_011189	2.51217	1.2955	
Akirin2	NM_001007589	2.38811	1.35509	
Tnfrsf11a	NM_009399	2.3389	1.26773	
Itgav	NM_008402	2.33464	1.18542	
Ddx3x	NM_010028	2.18403	1.22372	
Ifnk	NM_199157	2.07431	1.01507	
Adam9	NM_007404	1.99581	1.9453	
Wnt4	NM_009523	1.98006	1.46732	
Cnpy3	NM_028065	1.92469	1.3705	
Polr3e	NM_025298	1.90496	1.04829	
Psme2	ENSMUST00000104958	1.85701	1.87734	
Cd151	NM_009842	1.79999	1.30455	
Rps17	NM_009092	1.76317	1.13243	
Ireb2	NM_022655	1.75233	1.46103	
Hfe	NM_010424	1.73469	1.49071	

Trim25	NM_009546	1.72142	1.07456
Lcp2	ENSMUST00000169878	1.6707	5.26129
Ncor1	ENSMUST00000101066	1.65692	1.06599
Igbp1	NM_008784	1.65611	1.01096
Ptx3	NM_008987	1.61419	2.23212
Arhgef5	NM_133674	1.59546	1.01962
Ace	NM_207624	1.56921	1.43296
H60b	NM_001177775	1.56454	1.42547
Cklf	AF401531	1.5645	1.01826
Il18rap	NM_010553	1.5511	1.25655
Ifnab	NM_008336	1.53435	1.15731
Mpzl2	NM_007962	1.19224	1.53603
Dclre1c	NM_146114	1.16941	1.53843
Zbtb1	NM_178744	1.13292	1.50278
Treml2	NM_001033405	1.02233	1.9767
Axin1	NM_009733	-1.02653	-1.7137
Impdh2	NM_011830	-1.09053	-1.68852
Igbp1b	NM_015777	-1.50393	-1.00831
Nlrc3	NM_001081280	-1.5231	-1.18217
Ccr8	NM_007720	-1.53096	-1.09702
H2-Q10	ENSMUST00000174525	-1.54158	-1.29094
Wnt1	NM_021279	-1.54375	-1.24072
Ikbkg	NM_001136067	-1.55177	-1.10539
Tac4	NM_053093	-1.59519	-1.19084
Bag6	NM_057171	-1.62639	-1.19871
Prf1	NM_011073	-1.6397	-1.01514
Ifna7	NM_008334	-1.6449	-1.26737
Klrg1	NM_016970	-1.65945	-1.2494
Nlrx1	NM_178420	-1.67603	-1.23619
Ccr3	NM_009914	-1.68244	-1.23957
Ccnb2	NM_007630	-1.69335	-1.85622
Ccl25	ENSMUST00000024004	-1.69732	-1.04214
Mir18	NR_029736	-1.72055	-1.04069
Vav1	NM_011691	-1.7341	-1.09998
Fcamr	NM_001170632	-1.79761	-1.21435
Exosc5	NM_138586	-1.80247	-1.04595
Polr3h	NM_030229	-1.87398	-1.19855
Cxcr5	ENSMUST00000062215	-1.8786	-1.06505
Pfdn1	NM_026027	-1.96082	-1.15118
Tnfsf8	NM_009403	-2.08579	-1.32161
Ltb	NM_008518	-2.22741	-1.1425
Mir20a	NR_029737	-2.29769	-1.06964
Oas1b	NR_003507	-2.30545	-1.0265
Hist1h2ba	NM_175663	-2.45403	-1.03217

Nlrp3	NM_145827	-2.49225	-1.40218	
Aire	NM_009646	-2.59179	-1.15252	
Ifna12	NM_177361	-2.6592	-1.28773	
Il25	NM_080729	-2.70026	-1.12031	
Cd3d	NM_013487	-2.71109	-1.51753	
Sarm1	NM_001168521	-2.98593	-1.13337	
Osm	ENSMUST00000075221	-3.42782	-1.32258	
Rpl22	NM_009079	-3.49682	-1.23495	
Rps6ka3	NM_148945	10.5962	3.36536	innate immune response-activating signal transduction
Tlr13	NM_205820	5.25851	2.80314	
Lsm14a	NM_025948	2.49267	2.44574	
Tlr1	NM_030682	2.24246	1.52399	
Tnip3	NM_001001495	1.31189	2.67867	
Cd86	NM_019388	1.18013	2.26398	
Mapkapk3	NM_178907	-1.32766	-1.64164	
Anxa3	NM_013470	3.74125	2.87499	
Ccl3	NM_011337	3.27917	9.60407	
Dock2	NM_033374	1.58217	4.92041	
Myo1f	NM_053214	1.0234	1.82183	
Lgals8	NM_001199043	5.63143	1.1508	
Lcp1	NM_008879	4.3217	5.17435	
Psen1	NM_008943	2.4286	2.30243	
Gpr183	NM_183031	1.56216	1.09701	
Il18r1	NM_008365	1.44407	1.79136	
Icam1	NM_010493	1.15219	1.67931	
F2rl1	NM_007974	-1.7646	-1.7244	lymphocyte activation involved in immune response
Ifna4	NM_010504	-1.81564	-1.19279	
Apod	NM_007470	66.7312	1.88079	
Trim30a	NM_009099	22.3429	2.48677	
Vsig4	NM_177789	13.6254	1.31432	
Socs6	NM_018821	8.0847	1.91529	
Itch	NM_008395	4.95765	1.21405	
Peli1	NM_023324	3.8309	1.24203	
Ptprj	NM_008982	3.38957	3.03045	
Thbs1	NM_011580	3.37505	3.49767	
Cblb	NM_001033238	2.7621	1.46177	
Col3a1	NM_009930	2.5606	1.43784	
Nr1d1	NM_145434	1.95936	1.59486	
Trim27	NM_009054	1.57489	1.48626	
Elf1	NM_007920	1.56552	1.5362	
Psma1	NM_011965	1.51369	1.06771	
Mertk	NM_008587	1.47299	3.09424	
Id2	NM_010496	1.45911	1.66252	
Grem1	ENSMUST00000099575	-1.28343	-1.8929	

Tspan32	ENSMUST00000075172	-1.65206	-1.14263	
Dhx58	NM_030150	-1.67372	-1.22971	
Btla	NM_001037719	-1.89467	-1.39153	
Sh2d1b2	NM_001033499	-2.11738	-1.1112	
Trim38	NM_001029935	-2.11976	-1.18899	
Erbb2	NM_001003817	-2.26486	-1.20993	
Casp3	NM_009810	-3.28036	-1.0473	
Mgst1	NM_019946	5.9749	1.3022	peroxidase activity
Gpx8	NM_027127	5.46632	1.14281	
Cat	NM_009804	3.4342	2.02084	
Alox5ap	NM_009663	2.01433	3.36222	
Pxdn	NM_181395	1.76767	1.20692	
Mgst3	NM_025569	1.51937	1.07872	

References

[1] L.I. Huschtscha, C.E. Napier, J.R. Noble, K. Bower, A.Y.M. Au, H.G. Campbell, A.W. Braithwaite, R.R. Reddel. Enhanced isolation of fibroblasts from human skin explants. Biotechniques 53 (2012) 239-244.

[2] H.C. Chong, J.S.K. Chan, C.Q. Goh, N.V. Gounko, B. Luo, X. Wang, S. Foo, M.T.C. Wong, C. Choong, S. Kersten, N.S. Tan. Angiopoietin-like 4 stimulates STAT3-mediated iNOS expression and enhances angiogenesis to accelerate wound healing in diabetic mice. Mol Ther 22 (2014) 1593-1604.

[3] Y.Y. Goh, M. Pal, H.C. Chong, P. Zhu, M.J. Tan, L. Punugu, C.K. Tan, R.L. Huang, S.K. Sze, M.B.Y. Tang, J.L. Ding, S. Kersten, N.S. Tan. Angiopoietin-like 4 interacts with matrix proteins to modulate wound healing. J Biol Chem 285 (2010) 32999-33009.

[4] H.C. Chong, M.J. Tan, V. Philippe, S.H. Tan, C.K. Tan, C.W. Ku, Y.Y. Goh, W. Wahli, L. Michalik, N.S. Tan. Regulation of epithelial-mesenchymal IL-1 signaling by PPARbeta/delta is essential for skin homeostasis and wound healing. J Cell Biol 184 (2009) 817-831.